Force-enhancing vortex equilibria for two parallel plates in uniform flow

By Takashi SAKAJO

Department of mathematics, Hokkaido University, Sapporo, JAPAN
JST CREST
(sakajo@math.sci.hokudai.ac.jp)

A two-dimensional potential flow in an unbounded domain with two parallel plates is considered. We examine whether two free point vortices can be trapped near the two plates in the presence of a uniform flow and observe if these stationary point vortices enhance the force on the plates. The present study is an extension of the work by Saffman & Sheffield (1977), in which a free point vortex over a single plate is investigated. The flow problem is motivated by an airfoil design problem for the double wings. Moreover, it also contributes to a design problem for an efficient wind turbine with vertical blades. In order to obtain the point-vortex equilibria numerically, we make use of a linear algebraic algorithm combined with a stochastic process, called the Brownian ratchet scheme. The ratchet scheme allows us to capture a family of stationary point vortices in multiply connected domains with ease. As a result, we find that stationary point vortices exist around the two plates and they enhance the downward force and the counter-clockwise rotational force acting on the two plates.

Keywords: Point vortex equilibria; Multiply connected domains; Brownian ratchets

1. Introduction

Numerous researchers have suggested that the lift on an airfoil can be enhanced by trapping vortex structures around its wing. A well-known realisation of this idea is a delta wing, in which an additional lift is generated by placing a rolled-up vortex sheet separated from its leading edge (Hummel, 1978). Another example is known as "Kasper airfoil"(US patent #3831885), which is an airfoil design of a high aspect ratio wing with a flap proposed by Kasper. Kasper discussed a possibility to gain the lift by entrapping a free vortex around the wing. This concept was experimentally confirmed by Walton (1974) and Kruppa (1977) and found that it was not an easy task to maintain vortices around the wing stably. On the other hand, Rossow (1977) demonstrated that it was possible to keep a spanwise vortex line coupled with an axial flow along its core on the wing with a vertical flap.

In real viscous flows, even if the lift is enhanced by trapping vortices thanks to a flap, the increase of the drag is inevitable owing to the presence of the flap. Hence one would like to reduce the size of the flap as small as possible to reduce the drag. To deal with this problem, Saffman and Sheffield (1977) proposed a two-dimensional analytic model describing a free point vortex over a flat plate without any flap in the presence of a uniform flow, in which they showed the existence of stationary point vortices above the plate. Not only the stationary point vortices enhance the lift on the plate, but some of them are also stable with respect to two-dimensional disturbances.

On the other hand, Saffman & Sheffield (1977) pointed out that no stationary point vortex was obtained, if the Kutta condition was imposed both at the leading edge and the trailing edge simultaneously. To resolve this problem, two extensions of the analytic model have been made. Huang & Chow (1981) considered a point vortex over the Joukowski wing instead of the flat plate. Since the wing has no sharp leading edge, it is sufficient to impose the Kutta condition only at the trailing edge. Another extension was given by Mourtos & Brooks (1996). They considered a vortex-sink over a flat plate, which is a two-dimensional model of a spanwise vortex line with an axial flow. In this case, the stationary vortex-sink is uniquely determined even if the Kutta

condition is considered both at the leading and trailing edges. At any rate, all studies suggest the existence of stationary vortex structures enhancing the lift over the single wing in the uniform flow.

In the present paper, we consider the incompressible and inviscid flow in an unbounded plane as in Figure 1(b), in which two plates to be of equal length and slanted at the same angle ϕ to the x-axis are embedded. The centerpoints of the two plates are separated by the distances $\pm s$ from the origin. Identifying the unbounded plane with the complex z-plane, we refer to the exterior domain with the two parallel plates as D_z. Suppose that there exist a uniform flow of speed U parallel to the real axis and two point vortices of respective strengths κ_1 and κ_2 in the domain. If needed, we can also add circulations around the plates of strengths Γ_1 and Γ_2 respectively.

The present study is a geometric extension of the work by Saffman & Sheffield (1977) to a doubly connected domain, which is an airfoil model of the double wings. Moreover, it is also regarded as a two-dimensional model of a wind turbine, which is a wind-powered electronic generator with vertical two long blades. See the webpage at http://en.wikipedia.org/wiki/Vertical-axis_wind_turbine for a description of vertical axis wind turbines. When the uniform flow blows into these blades, it creates a rotational force on the blades, by which the electronic power is generated. With the same concept as the Kasper airfoil, we expect that stationary vortex lines attached to the blades enhance the rotational force. Thus it is important to find stationary configurations of the two point vortices around the two plates in the presence of the uniform flow and to investigate how the stationary point vortices enhance the force acting on the two plates.

The equations we need to solve in the present problem are described in terms of elliptic functions, since the flow domain with the two plates is a doubly connected domain. This poses some difficulties in solving for an equilibrium by numerical means, thus we introduce a simple linear algebraic approach, which is called the Brownian ratchet scheme. The numerical scheme was originally developed by Newton & Chamoun (2007) to obtain point-vortex equilibria in the plane. We show the numerical method is successfully applicable to the present problem.

The paper consists of six sections. In §2, we give a mathematical description of the flow problem following the calculus given by **?**. After explaining how to apply the Brownian ratchet scheme to the present problem in §3, we introduce in §4 a rigid rod model in order to discuss the force acting on the two plates. In §5, we show some examples of stationary point vortices around the plates and observe how these point-vortex equilibria enhance the force on the plates. The final section is conclusion and discussion.

2. Mathematical formulation

Solving the flow problem is a straightforward application of the calculus presented by Crowdy (2010). Let us first consider the annulus $\{\zeta \in \mathbb{C} \mid \rho < |\zeta| < 1\}$ in the complex ζ-plane. See Figure 1(a). This is a canonical doubly connected domain, for which explicit representation of the complex potential, say $W(\zeta)$, is available. Then constructing the conformal mapping $z = g(\zeta)$ from the annulus to the slit domain D_z, we obtain the required complex potentials by $W(g^{-1}(z))$, since the complex potential is conformally invariant.

The conformal mapping from the annulus to D_z is represented explicitly by the following form (Crowdy & Marshall, 2006).

$$g(\zeta) = A[K(\zeta/\sqrt{\rho}, \rho) - e^{2i\chi}K(\zeta\sqrt{\rho}, \rho) - K(-1, \rho) - \mathrm{e}^{2i\chi}K(-\rho, \rho)], \tag{2.1}$$

in which $\chi \in \mathbb{R}$ and $A \in \mathbb{C}$ are two parameters to be determined. The function $K(\zeta, \rho)$ is defined by

$$K(\zeta, \rho) = \frac{\zeta P_\zeta(\zeta, \rho)}{P(\zeta, \rho)},$$

in which $P(\zeta, \rho)$ is an elliptic function given by

$$P(\zeta, \rho) = (1 - \zeta)\prod_{k=1}^{\infty}(1 - \rho^{2k}\zeta)(1 - \rho^{2k}\zeta^{-1}),$$

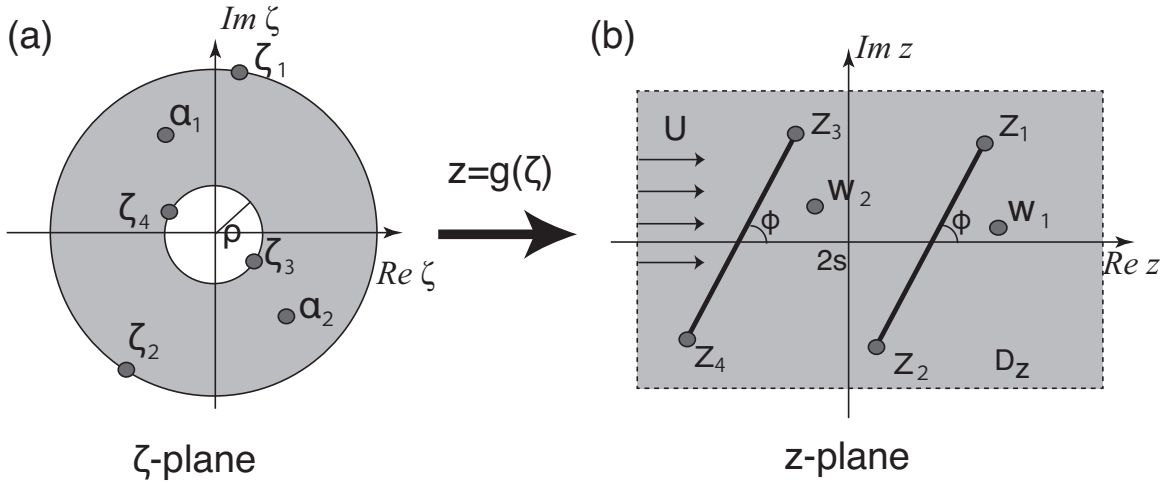

Figure 1. A schematic picture of the conformal mapping $z = g(\zeta)$. (a) A canonical annulus $\{\zeta \in \mathbb{C} \,|\, \rho < |\zeta| < 1\}$ in the complex ζ-plane. (b) A doubly connected exterior domain D_z with two parallel plates that are separated by the distance $2s$ and inclined at the angle ϕ to the real axis. The conformal mapping $z = g(\zeta)$ maps the boundaries of the annulus to the two slits of the exterior domain. The two point vortices located at α_1 and α_2 on the annulus are mapped to those at $w_1 = g(\alpha_1)$ and $w_2 = g(\alpha_2)$ in D_z respectively. The two points on the unit circle, ζ_1 and ζ_2, are mapped to the trailing edge $z_1 = g(\zeta_1)$ and the leading edge $z_2 = g(\zeta_2)$ of the right plate. The edges z_3, z_4 of the left plate are the images of the two points ζ_3 and ζ_4 on $|\zeta| = \rho$ in the annulus.

and $P_\zeta(\zeta, \rho)$ denotes the derivative with respect to the first argument. Note that the present form of $g(\zeta)$ ensures that the two points $\zeta = -\sqrt{\rho}$ and $\sqrt{\rho}$ in the annulus are mapped to 0 and ∞ in the domain D_z respectively. The boundaries of the annulus are also mapped to two equal size plates both of which are inclined at the same angle for all values of the parameters. The modulus of the multiplicative constant A can be chosen so that the plates are both unit length and their midpoints are centered on the real axis. With A determined in this way, the map depends on two parameters ρ and χ. These can be chosen so that the two plates are centered at the specified distance s from the origin and slanted at the specified angle ϕ. It is easy to find these parameters numerically through a Newton method for given s and ϕ. Hence, the distance $s > 0$ and the inclined angle $0 < \phi < \pi/2$ are the parameters we can choose freely in the present problem.

Suppose that two point vortices of strengths κ_1 and κ_2 are located at $\alpha_1(t)$ and $\alpha_2(t)$ at time t in the annulus. We note that the rotational direction generated by the point vortex is counter-clockwise when its strength is positive and vice versa, which is opposite from what Saffman & Sheffield (1977) used. Then the instantaneous complex potential in the annulus that describes the uniform flow of speed U and the two point vortices around the plates with circulations Γ_1 and Γ_2 in D_z is explicitly given by $W(\zeta, t) = W_U(\zeta) + W_V(\zeta, t) + W_0(\zeta) + W_\Gamma(\zeta)$, in which

$$\begin{aligned} W_U(\zeta) &= UA[K(\zeta/\sqrt{\rho}, \rho) - K(\zeta\sqrt{\rho}, \rho)], \\ W_V(\zeta, t) &= \kappa_1 G_0(\zeta, \alpha_1(t)) + \kappa_2 G_0(\zeta, \alpha_2(t)), \\ W_0(\zeta) &= -(\kappa_1 + \kappa_2) G_0(\zeta, \sqrt{\rho}), \\ W_\Gamma(\zeta) &= \frac{i(\Gamma_1 + \Gamma_2)}{2\pi} \log R_0(\zeta, \sqrt{\rho}) - \frac{i\Gamma_2}{2\pi} \log \zeta, \end{aligned}$$

where

$$G_0(\zeta, \gamma) = -\frac{i}{2\pi} \log\left(\frac{|\gamma| P(\zeta/\gamma, \rho)}{P(\zeta\gamma^*, \rho)}\right), \qquad R_0(\zeta, \gamma) = |\gamma|^2 \frac{P(\zeta/\gamma, \rho)}{P(\zeta\gamma^*, \rho)}, \qquad \zeta, \gamma \in \mathbb{C}.$$

Here, γ^* denotes the complex conjugate of $\gamma \in \mathbb{C}$. The complex potentials W_U and W_Γ represent the uniform flow and the flow due to circulation bound to the plate, whose explicit representations

are derived by Crowdy (2006). The second term W_V is the complex potential for the two point vortices, which is derived from the general form of the complex potential for a point vortex in multiply connected circular domains (Crowdy & Marshall, 2005). The complex potential W_0 represents a point vortex located at $\zeta = \sqrt{\rho}$ with the strength $-\kappa_1 - \kappa_2$. Thanks to the complex potential W_0, the branches of the logarithmic functions $W_V(\zeta, t)$ and $W_0(\zeta)$ coincide and they join $\alpha_1(t)$, $\alpha_2(t)$ and $\sqrt{\rho}$ in the annulus D_ζ. Consequently, they do not cross the boundaries of the annulus. Since $\zeta = \sqrt{\rho}$ is mapped to the infinity of D_z by the conformal mapping (2.1), the circulations around the two plates due to the point vortices become zero in D_z.

The derivative of the complex potential $W(\zeta)$ induces the complex conjugate of the velocity field, i.e., $\frac{\mathrm{d}W}{\mathrm{d}\zeta} = u - iv$, in which (u, v) denotes the velocity field. Thus, the complex potentials W_U, W_V, W_0 and W_Γ induce the following conjugate velocity field.

$$\frac{\mathrm{d}W_U}{\mathrm{d}\zeta}(\zeta) = \frac{UA}{\sqrt{\rho}}[K_\zeta(\zeta/\sqrt{\rho}, \rho) - \rho K_\zeta(\zeta\sqrt{\rho}, \rho)], \tag{2.2}$$

$$\frac{\mathrm{d}W_V}{\mathrm{d}\zeta}(\zeta) = -\frac{i}{2\pi\zeta}\sum_{\lambda=1}^{2}\kappa_\lambda[K(\zeta/\alpha_\lambda(t), \rho) - K(\zeta\alpha_\lambda^*(t), \rho)], \tag{2.3}$$

$$\frac{\mathrm{d}W_0}{\mathrm{d}\zeta}(\zeta) = \frac{i(\kappa_1 + \kappa_2)}{2\pi\zeta}\left(K(\zeta/\sqrt{\rho}, \rho) - K(\zeta\sqrt{\rho}, \rho)\right), \tag{2.4}$$

$$\frac{\mathrm{d}W_\Gamma}{\mathrm{d}\zeta}(\zeta) = \frac{i(\Gamma_1 + \Gamma_2)}{2\pi\zeta}(K(\zeta/\sqrt{\rho}, \rho) - K(\zeta\sqrt{\rho}, \rho)) - \frac{i\Gamma_2}{2\pi\zeta}. \tag{2.5}$$

The interaction between the two point vortices in the annulus is derived from the explicit representation of the N-vortex problem in multiply connected circular domains given by **?**, according to which the two point vortices induce the conjugate velocity field

$$I_1(t) = -\frac{i\kappa_2}{2\pi\alpha_1(t)}[K(\alpha_1(t)/\alpha_2(t), \rho) - K(\alpha_1(t)\alpha_2^*(t), \rho)] + \frac{i\kappa_1}{2\pi\alpha_1(t)}K(|\alpha_1(t)|^2, \rho), \tag{2.6}$$

at the position of the first point vortex, and

$$I_2(t) = -\frac{i\kappa_1}{2\pi\alpha_2(t)}[K(\alpha_2(t)/\alpha_1(t), \rho) - K(\alpha_2(t)\alpha_1^*(t), \rho)] + \frac{i\kappa_2}{2\pi\alpha_2(t)}K(|\alpha_2(t)|^2, \rho), \tag{2.7}$$

at the position of the second point vortex. Consequently, the equation of motion of the two point vortices $\alpha_m(t)$ in the annulus is given by

$$\frac{\mathrm{d}\alpha_m^*}{\mathrm{d}t} = \frac{\mathrm{d}W_U}{\mathrm{d}\zeta}(\alpha_m(t)) + I_m(t) + \frac{\mathrm{d}W_0}{\mathrm{d}\zeta}(\alpha_m(t)) + \frac{\mathrm{d}W_\Gamma}{\mathrm{d}\zeta}(\alpha_m(t)), \qquad m = 1, 2.$$

On the use of Routh's correction, we modify the equation with the conformal mapping $z = g(\zeta)$ (Saffman, 1992). Thus the equation of motion for the two point vortices at $w_m = g(\alpha_m)$ in the slit domain D_z is given by

$$\frac{\mathrm{d}w_m^*}{\mathrm{d}t} = \frac{1}{g_\zeta(\alpha_m)}\left(\frac{\mathrm{d}\alpha_m^*}{\mathrm{d}t} + \frac{i\kappa_m}{4\pi}\frac{g_{\zeta\zeta}(\alpha_m)}{g_\zeta(\alpha_m)}\right). \tag{2.8}$$

Hence, the point vortices at w_1 and w_2 in the domain D_z are stationary when the pre-image point vortices at α_1 and α_2 in the annulus satisfy

$$\frac{\mathrm{d}W_U}{\mathrm{d}\zeta}(\alpha_m) + I_m + \frac{\mathrm{d}W_0}{\mathrm{d}\zeta}(\alpha_m) + \frac{\mathrm{d}W_\Gamma}{\mathrm{d}\zeta}(\alpha_m) + \frac{i\kappa_m}{4\pi}\frac{g_{\zeta\zeta}(\alpha_m)}{g_\zeta(\alpha_m)} = 0, \qquad m = 1, 2. \tag{2.9}$$

In order to avoid a velocity singularity, we need to impose the Kutta condition at the edge of the plate. Let z_1, z_2, z_3 and z_4 represent the locations of the trailing edges and the leading edges of the two plates in D_z. Their pre-images at the boundaries of the annulus D_ζ are denoted by ζ_m, namely they satisfy $g(\zeta_m) = z_m$. See Figure 1(a) and (b) for their configurations. Note that

z_m and ζ_m are well-defined by the conformal mapping for $0 < \phi < \pi/2$, since the pre-image do not lie on the imaginary axis. Then the Kutta condition at ζ_m is described by

$$\mathrm{Im}\left(\frac{\mathrm{d}W}{\mathrm{d}\zeta}(\zeta_m)\right) = \mathrm{Im}\left(\frac{\mathrm{d}W_U}{\mathrm{d}\zeta}(\zeta_m) + \frac{\mathrm{d}W_V}{\mathrm{d}\zeta}(\zeta_m) + \frac{\mathrm{d}W_0}{\mathrm{d}\zeta}(\zeta_m) + \frac{\mathrm{d}W_\Gamma}{\mathrm{d}\zeta}(\zeta_m)\right) = 0. \tag{2.10}$$

It provides us with an additional real equation. Note that it is sufficient for us to consider the Kutta condition in terms of the imaginary part, since the normal condition on the two concentric boundaries of the annulus is automatically satisfied by the condition.

Plugging (2.2) – (2.7) into the conditions (2.9) and (2.10), we have the equations to be solved. The two point vortices at α_1 and α_2 are stationary, if they satisfy

$$\frac{UA}{\sqrt{\rho}}[K_\zeta(\alpha_1/\sqrt{\rho},\rho) - \rho K_\zeta(\alpha_1\sqrt{\rho},\rho)] + \frac{i(\kappa_1+\kappa_2+\Gamma_1+\Gamma_2)}{2\pi\alpha_1}[K(\alpha_1/\sqrt{\rho},\rho) - K(\alpha_1\sqrt{\rho},\rho)]$$
$$-\frac{i\Gamma_2}{2\pi\alpha_1} - \frac{i\kappa_2}{2\pi\alpha_1}[K(\alpha_1/\alpha_2,\rho) - K(\alpha_1\alpha_2^*,\rho)] + \frac{i\kappa_1}{2\pi\alpha_1}K(|\alpha_1|^2,\rho) + \frac{i\kappa_1}{4\pi}\frac{g_{\zeta\zeta}(\alpha_1)}{g_\zeta(\alpha_1)} = 0, \tag{2.11}$$

$$\frac{UA}{\sqrt{\rho}}[K_\zeta(\alpha_2/\sqrt{\rho},\rho) - \rho K_\zeta(\alpha_2\sqrt{\rho},\rho)] + \frac{i(\kappa_1+\kappa_2+\Gamma_1+\Gamma_2)}{2\pi\alpha_2}[K(\alpha_2/\sqrt{\rho},\rho) - K(\alpha_2\sqrt{\rho},\rho)]$$
$$-\frac{i\Gamma_2}{2\pi\alpha_2} - \frac{i\kappa_1}{2\pi\alpha_2}[K(\alpha_2/\alpha_1,\rho) - K(\alpha_2\alpha_1^*,\rho)] + \frac{i\kappa_2}{2\pi\alpha_2}K(|\alpha_2|^2,\rho) + \frac{i\kappa_2}{4\pi}\frac{g_{\zeta\zeta}(\alpha_2)}{g_\zeta(\alpha_2)} = 0, \tag{2.12}$$

which correspond to four real equations. Let us note that the number of the real unknowns in the present problem is eight, which are the locations of the two point vortices $\alpha_1,\ \alpha_2 \in \mathbb{C}$, their strengths $\kappa_1,\ \kappa_2 \in \mathbb{R}$, and the circulations $\Gamma_1,\ \Gamma_2 \in \mathbb{R}$ around the two plates. Hence, one can consider the Kutta condition at four edges to make the number of the equations the same. On the other hand, the existence of a vortex equilibrium satisfying the Kutta conditions at sharp edges is a subtle issue. For instance, Zannetti (2006) pointed out that, in some cases, no point-vortex equilibrium is found when the Kutta condition is imposed at a certain edge. In the present problem, as we see in Saffman & Sheffield (1977), no vortex equilibrium exists when we consider the Kutta condition at all edges of the plates simultaneously. Thus, we consider the Kutta conditions at three edges. There are four possibilities to choose three edges out of the four, but there is no particular reason which to choose from a physical point of view. In principle, it is necessary to consider all choices of three edges, if we want to find optimal configurations of point-vortex equilibria that enhance the force better. However, in the present paper, we impose the Kutta conditions at the three edges ζ_1, ζ_2 and ζ_3 as a test case, which are explicitly described as follows.

$$\mathrm{Im}\left(\frac{UA}{\sqrt{\rho}}[K_\zeta(\zeta_1/\sqrt{\rho},\rho) - \rho K_\zeta(\zeta_1\sqrt{\rho},\rho)] - \frac{i}{2\pi\zeta_1}\sum_{\lambda=1}^{2}\kappa_\lambda[K(\zeta_1/\alpha_\lambda,\rho) - K(\zeta_1\alpha_\lambda^*,\rho)]\right.$$
$$\left.+\frac{i(\kappa_1+\kappa_2+\Gamma_1+\Gamma_2)}{2\pi\zeta_1}[K(\zeta_1/\sqrt{\rho},\rho) - K(\zeta_1\sqrt{\rho},\rho)] - \frac{i\Gamma_2}{2\pi\zeta_1}\right) = 0, \tag{2.13}$$

$$\mathrm{Im}\left(\frac{UA}{\sqrt{\rho}}[K_\zeta(\zeta_2/\sqrt{\rho},\rho) - \rho K_\zeta(\zeta_2\sqrt{\rho},\rho)] - \frac{i}{2\pi\zeta_2}\sum_{\lambda=1}^{2}\kappa_\lambda[K(\zeta_2/\alpha_\lambda,\rho) - K(\zeta_2\alpha_\lambda^*,\rho)]\right.$$
$$\left.+\frac{i(\kappa_1+\kappa_2+\Gamma_1+\Gamma_2)}{2\pi\zeta_2}[K(\zeta_2/\sqrt{\rho},\rho) - K(\zeta_2\sqrt{\rho},\rho)] - \frac{i\Gamma_2}{2\pi\zeta_2}\right) = 0, \tag{2.14}$$

$$\mathrm{Im}\left(\frac{UA}{\sqrt{\rho}}[K_\zeta(\zeta_3/\sqrt{\rho},\rho) - \rho K_\zeta(\zeta_3\sqrt{\rho},\rho)] - \frac{i}{2\pi\zeta_3}\sum_{\lambda=1}^{2}\kappa_\lambda[K(\zeta_3/\alpha_\lambda,\rho) - K(\zeta_3\alpha_\lambda^*,\rho)]\right.$$
$$\left.+\frac{i(\kappa_1+\kappa_2+\Gamma_1+\Gamma_2)}{2\pi\zeta_3}[K(\zeta_3/\sqrt{\rho},\rho) - K(\zeta_3\sqrt{\rho},\rho)] - \frac{i\Gamma_2}{2\pi\zeta_3}\right) = 0. \tag{2.15}$$

The equations (2.11) – (2.15) are the seven real nonlinear equations for the eight unknowns α_1, α_2, κ_1, κ_2, Γ_1 and Γ_2 for a given speed of the uniform flow U. Consequently, solutions of the

nonlinear equations form a one-dimensional family of the point-vortex equilibria, which will be examined by numerical means.

3. Numerical methods

The nonlinear equations (2.11) – (2.15) can be solved numerically with a standard Newton-Raphson method in principle, but we introduce a simpler linear algebraic approach, called the Brownian ratchet scheme. Let us regard the speed of the uniform flow U as a real unknown at the moment, whose value is properly determined to obtain a unique solution later. Then the equations depend linearly on the speed of the uniform flow U, the vortex strengths κ_1, κ_2, and the round-plate circulations Γ_1, Γ_2, when the locations of the two point vortices α_1 and α_2 are fixed. Therefore, for a given configuration of the two point vortices, the equations (2.11) – (2.15) can be regarded as a linear equations $\mathcal{A}\boldsymbol{x} = \boldsymbol{0}$ for the 7×5 matrix $\mathcal{A}$ and $\boldsymbol{x} = (U, \kappa_1, \kappa_2, \Gamma_1, \Gamma_2)^T$. Each component of the matrix

$$\mathcal{A} = \begin{pmatrix} A_0 & A_7 & A_{14} & A_{21} & A_{28} \\ A_1 & A_8 & A_{15} & A_{22} & A_{29} \\ A_2 & A_9 & A_{16} & A_{23} & A_{30} \\ A_3 & A_{10} & A_{17} & A_{24} & A_{31} \\ A_4 & A_{11} & A_{18} & A_{25} & A_{32} \\ A_5 & A_{12} & A_{19} & A_{26} & A_{33} \\ A_6 & A_{13} & A_{20} & A_{27} & A_{34} \end{pmatrix},$$

is represented by

$$A_0+iA_1 = \mathcal{F}(\alpha_1), \quad A_2+iA_3 = \mathcal{F}(\alpha_2), \quad A_4 = \mathrm{Im}(\mathcal{F}(\zeta_1)), \quad A_5 = \mathrm{Im}(\mathcal{F}(\zeta_2)), \quad A_6 = \mathrm{Im}(\mathcal{F}(\zeta_3)),$$

$$\begin{aligned} A_7 + iA_8 &= \mathcal{K}(\alpha_1, \sqrt{\rho}) + \frac{i}{2\pi\alpha_1} K(|\alpha_1|^2, \rho) + \frac{i}{4\pi}\frac{g_{\zeta\zeta}(\alpha_1)}{g_\zeta(\alpha_1)}, \\ A_9 + A_{10} &= \mathcal{K}(\alpha_2, \sqrt{\rho}) - \mathcal{K}(\alpha_2, \alpha_1), \end{aligned}$$

$$A_{11} = \mathrm{Im}(\mathcal{K}(\zeta_1, \sqrt{\rho}) - \mathcal{K}(\zeta_1, \alpha_1)), \quad A_{12} = \mathrm{Im}(\mathcal{K}(\zeta_2, \sqrt{\rho}) - \mathcal{K}(\zeta_2, \alpha_1)), \quad A_{13} = \mathrm{Im}(\mathcal{K}(\zeta_3, \sqrt{\rho}) - \mathcal{K}(\zeta_3, \alpha_1)),$$

$$\begin{aligned} A_{14} + iA_{15} &= \mathcal{K}(\alpha_1, \sqrt{\rho}) - \mathcal{K}(\alpha_1, \alpha_2), \\ A_{16} + iA_{17} &= \mathcal{K}(\alpha_2, \sqrt{\rho}) + \frac{i}{2\pi\alpha_2} K(|\alpha_2|^2, \rho) + \frac{i}{4\pi}\frac{g_{\zeta\zeta}(\alpha_2)}{g_\zeta(\alpha_2)}, \end{aligned}$$

$$A_{18} = \mathrm{Im}(\mathcal{K}(\zeta_1, \sqrt{\rho}) - \mathcal{K}(\zeta_1, \alpha_2)), \quad A_{19} = \mathrm{In}(\mathcal{K}(\zeta_2, \sqrt{\rho}) - \mathcal{K}(\zeta_2, \alpha_2)), \quad A_{20} = \mathrm{In}(\mathcal{K}(\zeta_3, \sqrt{\rho}) - \mathcal{K}(\zeta_3, \alpha_2)),$$

$$A_{21} + iA_{22} = \mathcal{K}(\alpha_1, \sqrt{\rho}), \qquad A_{23} + iA_{24} = \mathcal{K}(\alpha_2, \sqrt{\rho}),$$

$$A_{25} = \mathrm{Im}(\mathcal{K}(\zeta_1, \sqrt{\rho})), \qquad A_{26} = \mathrm{Im}(\mathcal{K}(\zeta_2, \sqrt{\rho})), \qquad A_{27} = \mathrm{Im}(\mathcal{K}(\zeta_3, \sqrt{\rho})),$$

$$A_{28} + iA_{29} = \mathcal{K}(\alpha_1, \sqrt{\rho}) - \frac{i}{2\pi\alpha_1}, \qquad A_{30} + iA_{31} = \mathcal{K}(\alpha_2, \sqrt{\rho}) - \frac{i}{2\pi\alpha_2},$$

$$A_{32} = \mathrm{Im}\left(\mathcal{K}(\zeta_1, \sqrt{\rho}) - \frac{i}{2\pi\zeta_1}\right), \quad A_{33} = \mathrm{Im}\left(\mathcal{K}(\zeta_2, \sqrt{\rho}) - \frac{i}{2\pi\zeta_2}\right), \quad A_{34} = \mathrm{Im}\left(\mathcal{K}(\zeta_3, \sqrt{\rho}) - \frac{i}{2\pi\zeta_3}\right),$$

in which the two functions $\mathcal{F}(\zeta)$ and $\mathcal{K}(\zeta_1, \zeta_2)$ are defined by

$$\mathcal{F}(\zeta) = \frac{A}{\sqrt{\rho}}[K_\zeta(\zeta/\sqrt{\rho}, \rho) - \rho K_\zeta(\zeta\sqrt{\rho}, \rho)], \qquad \mathcal{K}(\zeta_1, \zeta_2) = \frac{i}{2\pi\zeta_1}[K(\zeta_1/\zeta_2, \rho) - K(\zeta_1\zeta_2^*, \rho)].$$

Since all components of the matrix $\mathcal{A}$ are computable once the positions of the two point vortices α_1 and α_2 in the annulus are provided, we call the matrix *the configuration matrix for* α_1 *and* α_2. In general, the matrix $\mathcal{A}$ is not rank deficient when we choose the locations of the point

vortices arbitrarily. However, if we could find the locations of the two point vortices for which the configuration matrix $\mathcal{A}$ satisfies $\det(\mathcal{A}^T\mathcal{A}) = 0$, then the matrix would be rank deficient and it has a non-trivial null-space. Moreover, the linear basis for the null-space of $\mathcal{A}$ is obtained by the singular value decomposition of the configuration matrix (Trefethern & Bau III, 1997). That is to say, we solve the linear equations,

$$\mathcal{A}\boldsymbol{v}_i = \sigma_i \boldsymbol{u}_i, \qquad \mathcal{A}^T\boldsymbol{u}_i = \sigma_i \boldsymbol{v}_i, \qquad i = 1, \dots 5,$$

in which $\sigma_1 \geq \sigma_2 \geq \cdots \geq \sigma_5 \geq 0$ are the singular values, and $\boldsymbol{u}_i$ and $\boldsymbol{v}_i$ are the left and the right singular vectors corresponding to the singular value σ_i. In the Brownian ratchet scheme, we look for locations of two point vortices whose configuration matrix has a one-dimensional null-space, i.e., $\sigma_4 \neq 0$ and $\sigma_5 = 0$. Then the right singular vector $\boldsymbol{v}_5$ to the zero singular value σ_5 is the linear basis of a one-dimensional null space for the linear equation $\mathcal{A}\boldsymbol{x} = \boldsymbol{0}$, namely $\boldsymbol{x} \in \mathrm{Span}\langle \boldsymbol{v}_5 \rangle$. In order to obtain a unique solution for the linear equation, the vector $\boldsymbol{x}$ in the null space is normalized so that its first component U becomes the unity. The normalisation is appropriate, since the speed of the uniform flow can be chosen as $U = 1$ without loss of generality. Here is the description of the Brownian ratchet scheme:

Step 1 (Initialization) We give an initial guess α_1 and α_2 for the positions of two point vortices, and compute the smallest singular value σ_5 of the configuration matrix for α_1 and α_2. Then we set $\sigma_{min} = \sigma_5$.

Step 2 Repeat the following steps until σ_{min} gets smaller than 1.0×10^{-13}:

- Let the two points move freely with the Gaussian random walk of the variance σ_{min} to obtain new points at $\widetilde{\alpha}_1$ and $\widetilde{\alpha}_2$.
- We compute the smallest singular value $\widetilde{\sigma}_5$ of the configuration matrix for $\widetilde{\alpha}_1$ and $\widetilde{\alpha}_2$.
- If $\widetilde{\sigma}_5 \leq \sigma_{min}$ then we renew the locations of the two points, i.e., $\alpha_1 = \widetilde{\alpha}_1$ and $\alpha_2 = \widetilde{\alpha}_2$, and reset the variance of the Gaussian random walk to $\sigma_{min} = \widetilde{\sigma}_5$. Otherwise we discard the trial.

Step 3 If converged, the Brownian ratchet scheme ensures that the smallest singular value of the configuration matrix for α_1 and α_2 is less than 1.0×10^{-13}. Thus the two point vortices located at α_1 and α_2 become an equilibrium. Moreover, each component of the normalised right singular vector corresponding to σ_{min} gives the speed of the uniform flow $U = 1$, the strengths of the point vortices κ_1, κ_2, and of the round-plate circulations Γ_1, Γ_2 respectively.

In the first step of the algorithm, we must choose the initial guess for the positions of two point vortices so that the smallest singular value of the configuration matrix becomes as sufficiently small as possible. Indeed the Brownian ratchet scheme hardly converges when the two point vortices are set randomly in the annulus. This is because the annulus is mapped to the unbounded domain D_z with the two slits by the conformal mapping $g(\zeta)$, and so it is less probable for the two point vortices to be located in the neighborhood of the fixed configuration. Thus we search the initial guess near the leading edges and the trailing edges of the two plates in the following way.

Considering a circle of a small radius ϵ_m around the pre-image ζ_m of the edge, we generate a set of $K \times L$ grid points $\beta^{(m)} = \left\{ \beta_{k,l}^{(m)} \right\}$ in the polar coordinates, in which

$$\beta_{k,l}^{(m)} = \zeta_m + \epsilon_m \frac{k}{K} \exp\left(2\pi i \frac{l}{L} \right), \tag{3.1}$$

for $k = 1, \dots, K$ and $l = 0, \dots, L-1$. Since the center of the circle ζ_m is on the boundary of the annulus, some grid points are located outside of the annulus. Since these grid points are not mapped in D_z by the conformal mapping, we remove them from the set $\beta^{(m)}$. Then, we consider the four pairs of the sets of grid points that are mapped around the edges of the two plates by

the conformal mapping, say $\left(\beta^{(1)},\beta^{(3)}\right)$, $\left(\beta^{(2)},\beta^{(4)}\right)$, $\left(\beta^{(2)},\beta^{(3)}\right)$ and $\left(\beta^{(1)},\beta^{(4)}\right)$, from which we choose the initial guess of the Brownian ratchet scheme.

Let us describe how to choose the initial guess of the Brownian ratchet scheme from the sets $\left(\beta^{(1)},\beta^{(3)}\right)$ for instance. The initial guess for the other cases is also obtained in the same way. For fixed k, we compute the smallest singular values, say $\sigma_5^{(k)}(l,m,n)$, of the configuration matrix for $\beta^{(1)}_{k,l} \in \beta^{(1)}$ and $\beta^{(3)}_{m,n} \in \beta^{(3)}$ for all $l,n = 0,\ldots,L-1$ and $m = 1,\ldots,K$. Then we determine the initial guess of the locations of two point vortices, say $\alpha_1 = \beta^{(1)}_{k,l_k}$ and $\alpha_2 = \beta^{(3)}_{m_k,n_k}$, so that $\sigma_5^{(k)}(l_k,m_k,n_k)$ becomes the smallest. In other words, the triple of integers (l_k,m_k,n_k) is represented by

$$(l_k,m_k,n_k) = \mathrm{argmin}_{(l,m,n)}\, \sigma_5^{(k)}(l,m,n).$$

Repeating this procedure for $k = 1,\ldots,K$, we obtain K initial guesses for the Brownian ratchet scheme. In the present numerical computation, for $s = 0.6$, the value of the radius in (3.1) is given by $\epsilon_m = 0.85\times(1-\sqrt{\rho})$ for the trailing edges ζ_1, ζ_3 and $\epsilon_m = 0.5\times(\sqrt{\rho}-\rho)$ for the leading edges ζ_2, ζ_4. The grid points in $\beta^{(m)}$ are generated with $K = 150$ and $L = 300$.

Figure 2(a) shows a family of point-vortex equilibria for $s = 0.6$ and $\phi = 0.8$ computed by the Brownian ratchet scheme starting with the initial guesses chosen from the grid points in $\left(\beta^{(2)},\beta^{(3)}\right)$. We observe that the stationary two point vortices form two continuous loci. One locus lies behind the left plate and the other locus reaches the leading edge of the right plate, whose enlarged plots are shown in Figure 2(b) and (c) respectively. We draw the symbols $\circ$ and $\square$ at both endpoints of the loci to see the correspondence of the two stationary point vortices, which indicate that the pair of the fixed point vortices moves continuously along the loci from the configuration of the $\circ$ symbols to that of the $\square$ symbols. Let us note that the $\square$ symbols are just drawn for the sake of convenience and they are not true endpoints of the loci. The loci can be extended beyond the $\square$ points if we take different initial guesses. The enlarged plots also show that the distribution of the point vortices in the loci is non-uniform, which is due to the stochastic nature of the Brownian ratchet scheme. As we see in § 5, since all loci obtained in the present paper are connected to the edge of the right plate, we make use of the arclength of the right locus measured from the edge as a parameter to identify the location of the point-vortex equilibria in the loci and to describe numerical results.

4. Forces on the two plates

Let $C_0 : |\zeta| = 1$ and $C_1 : |\zeta| = \rho$ denote the two boundaries of the annulus D_ζ. Then the force $\left(F_x^{(m)},F_y^{(m)}\right)$ acting on the two plates $g(C_m)$ in the doubly connected slit domain D_z is obtained by using the Blasius formula:

$$F_x^{(m)} - iF_y^{(m)} = \frac{i}{2}\int_{C_m}\left(\frac{dW}{d\zeta}(\zeta)\right)^2\left(\frac{d\zeta}{dz}\right)d\zeta = \frac{i}{2}\int_{C_m}\left(\frac{dW}{d\zeta}(\zeta)\right)^2\frac{d\zeta}{g_\zeta(\zeta)}, \qquad m = 0,1,$$

which is computed numerically by the trapezoidal rule.

Here we propose a *rigid rod* model to discuss the force acting on the two plates, in which we assume that the centerpoints of the two plates are connected by an infinitely thin rigid rod along the x-axis. We also assume that the forces $F^{(0)}$ and $F^{(1)}$ act at the centerpoints of the two plates, which are the endpoints of the rigid rod. See Figure 3 for a schematic picture of the model. Then decomposing the components of $F^{(0)}$ and $F^{(1)}$ in the x and y-directions, we define the following four forces:

- $F_L = F_y^{(0)} + F_y^{(1)}$ is the lift in the y-direction, which represents an upward force if $F_L > 0$ and a downward force if $F_L < 0$.
- $F_R = F_y^{(0)} - F_y^{(1)}$ rotates the rod in the counter-clockwise direction for $F_R > 0$ and the clockwise direction for $F_R < 0$.

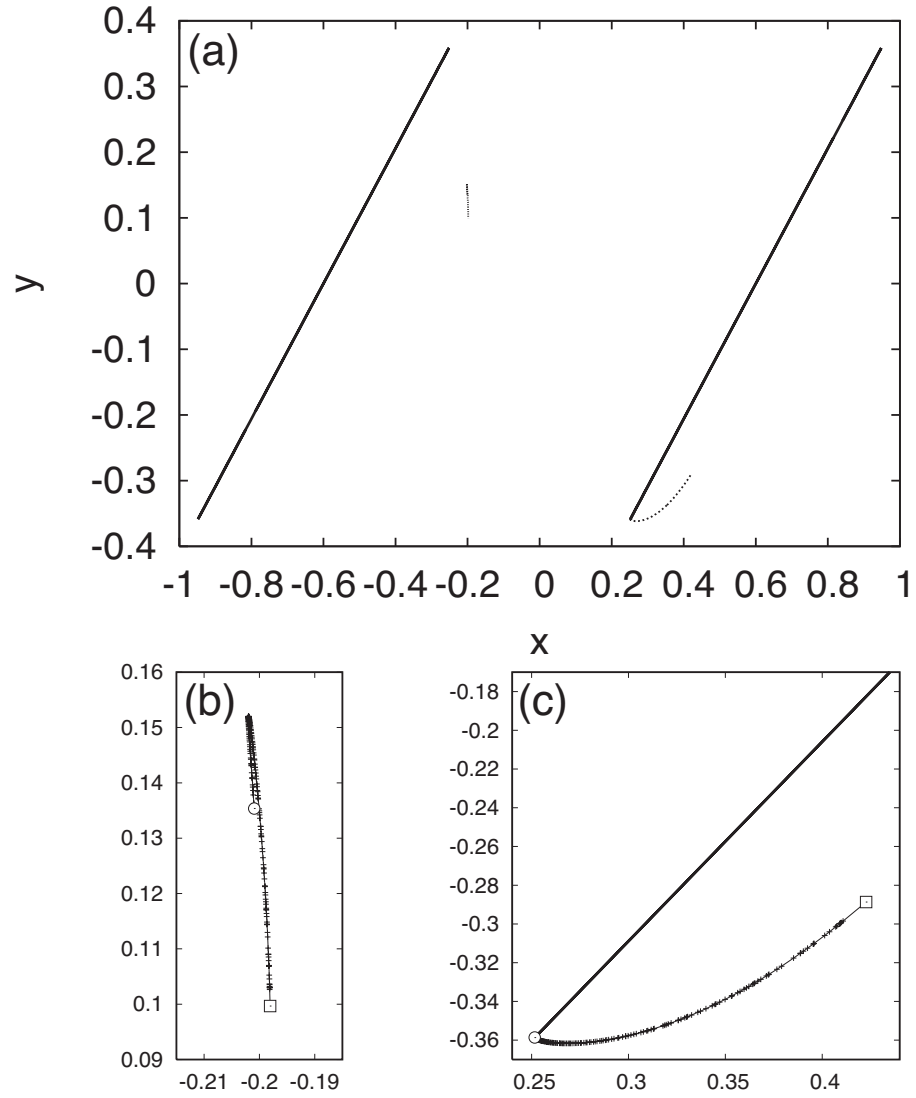

Figure 2. (a) Fixed configurations of the two point vortices around the two plates for $s = 0.6$ and $\phi = 0.8$. They are computed by the Brownian ratchet scheme starting with the initial guesses chosen from the grid points in $\left(\beta^{(1)}, \beta^{(3)}\right)$. (b) Enlarged plot of the left locus. (c) Enlarged plot of the right locus. The symbols $\circ$ and $\square$ represent the pairs of stationary point vortices located at the endpoints of the two loci.

- $F_D = F_x^{(0)} + F_x^{(1)}$ represents the drift force in the x-direction, which is a downstream force for $F_D > 0$ and an upstream force for $F_D < 0$.
- $F_I = F_x^{(0)} - F_x^{(1)}$ is the force between the two parallel plates, which is repulsive for $F_I > 0$ and attractive for $F_I < 0$.

In the present paper, we are interested in the lift F_L and the rotational force F_R in particular, since they are important in the application of the double wings and the wind turbine with vertical blades. We compute the forces by using the point-vortex equilibria with the strengths κ_1, κ_2 and the round-plate circulations Γ_1, Γ_2, which are denoted by $F_L^{(v)}$ and $F_R^{(v)}$. For the sake of comparison, we compute the forces without the point-vortex equilibria with keeping the round-plate circulations the same, which are denoted by $F_L^{(o)}$ and $F_R^{(o)}$. In principle, the values of the round-plate circulations can be arbitrarily chosen if there exists no stationary point vortex, but we keep these values unchanged to observe the force enhancements due to the existence of point-

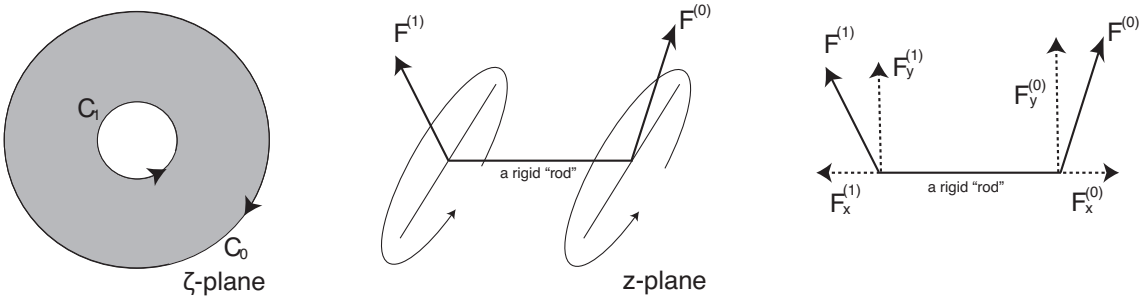

Figure 3. A rigid rod model of the forces acting on the two parallel plates.

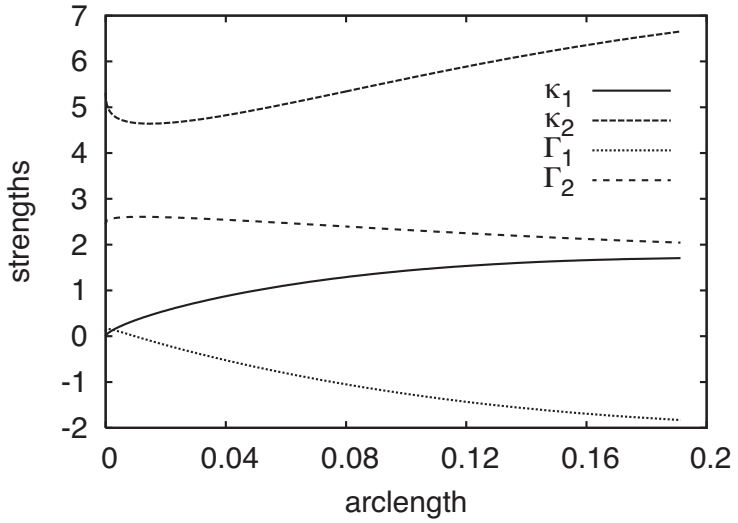

Figure 4. Plots of the strengths of the two point vortices κ_1, κ_2 and of the circulations around the plates Γ_1, Γ_2 corresponding to the point-vortex equilibria for $s = 0.6$ and $\phi = 0.8$.

vortex equilibria. Then the differences $\Delta F_L = F_L^{(v)} - F_L^{(o)}$ and $\Delta F_R = F_R^{(v)} - F_R^{(o)}$ indicate how the stationary point-vortex equilibria change the forces on the rigid rod.

5. Point-vortex equilibria and force enhancements

(*a*) *Fixed point vortices for* $s = 0.6$ *and* $\phi = 0.8$

Let us first consider a case when the distance between the two plates is $s = 0.6$ and their inclined angle is $\phi = 0.8$, for which we compute the point-vortex equilibria and observe how they enhance the lift and the rotational force acting on the two plates. The loci of the point-vortex equilibria for this case have been plotted in Figure 2(a). Figure 4 shows their corresponding point-vortex strengths κ_1, κ_2 and the round-plate circulations Γ_1, Γ_2 respectively. The initial guesses of the Brownian ratchet scheme are picked up from $\left(\beta^{(2)}, \beta^{(3)}\right)$. The point-vortex strengths and the round-plate circulations in Figure 4 are parametrised by the arclength of the right locus. As the point vortex in the right locus is away from the leading edge, its strength κ_1 monotonically increases from zero and the circulation Γ_1 around the right plate decreases and becomes negative. On the other hand, both the vortex strength κ_2 in the left locus and the circulation Γ_2 around the left plate are positive, while κ_2 attains the minimum and Γ_2 does the maximum when the point vortex in Figure 2(b) is located at the turning point in the middle of the left locus.

Figure 5(a) and (b) show the lifts $F_L^{(v)}$, $F_L^{(o)}$ and ΔF_L, and the rotational forces $F_R^{(v)}$, $F_R^{(o)}$

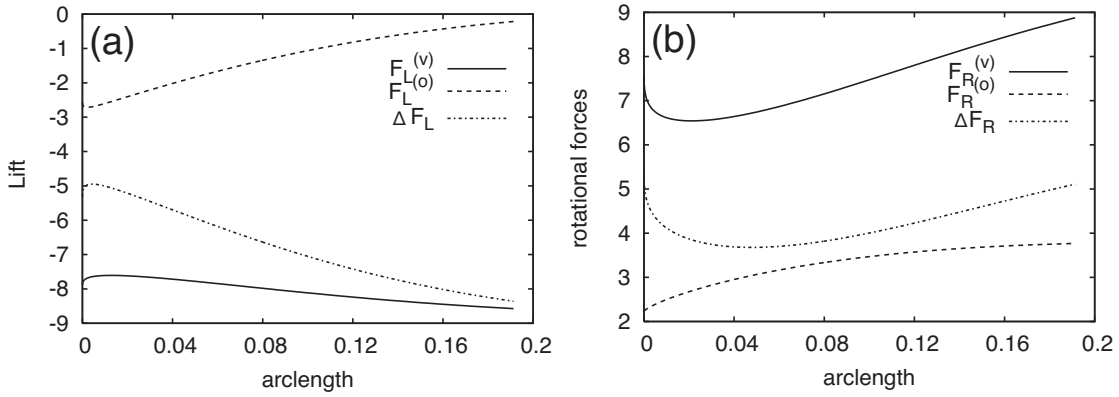

Figure 5. (a) Plot of the lifts $F_L^{(v)}$, $F_L^{(o)}$ and their difference ΔF_L. (b) Plots of the rotational forces $F_R^{(v)}$, $F_R^{(o)}$ and their difference ΔF_R. They are computed for the point-vortex equilibria in Figure 2(a)

.

and ΔF_R respectively. Without the point-vortex equilibria, the lift $F_L^{(o)} < 0$ is downward and the rotational force $F_R^{(o)} > 0$ is counter-clockwise. On the other hand, we observe $\Delta F_L < 0$ and $\Delta F_R > 0$ for all the equilibria due to $F_L^{(v)} < F_L^{(o)}$ and $F_R^{(v)} > F_R^{(o)}$. This indicates that the downward force and the counter-clockwise rotation are enhanced by the existence of the point-vortex equilibria. The maximum enhancement of the downward force and the rotational force is attained when the point vortex in the right locus is located at the farthest point from the leading edge, which corresponds to the vortex pair represented by the $\square$ symbols in Figure 2(b) and (c).

We compute the loci of the point-vortex equilibria for $s = 0.6$ and $\phi = 0.8$ when the Brownian ratchet scheme starts with the other initial guess. Figure 6(a), (b) and (c) show the loci of the point-vortex equilibria for the initial guesses taken from $\left(\beta^{(1)}, \beta^{(3)}\right)$, $\left(\beta^{(2)}, \beta^{(4)}\right)$ and $\left(\beta^{(1)}, \beta^{(4)}\right)$ respectively. Their corresponding vortex strengths and the round-plate circulations are plotted in Figure 6(d), (e) and (f). For the loci of Figure 6(a), one locus is connected to the trailing edge of the right plate, while the other small locus lies behind the left plate. Figure 6(d) indicates that the strength κ_1 of the point vortex in the right locus is positive and increases as the point vortex goes away from the trailing edge. The strength κ_2 of the point vortex in the left locus is always larger than that in the right locus. The round-plate circulations satisfy $\Gamma_1 < 0 < \Gamma_2$. Regarding the loci of the point-vortex equilibria in Figure 6(b) and Figure 6(c), the right locus joins the edge of the plate, whereas the left locus is located far beneath the leading edge of the plate. Both the vortex strengths and the round-plate circulations satisfy $0 < \kappa_1 < \kappa_2$ and $\Gamma_2 < \Gamma_1$ as we see in Figure 6(e) and (f).

Figure 7(a) and (b) are the plots of the lift enhancement ΔF_L and the rotational force enhancement ΔF_R computed for the point-vortex equilibria shown in Figure 6. They indicate that the point-vortex equilibria enhance the downward force and the counter-clockwise rotation for all cases, since we have $\Delta F_L < 0$ and $\Delta F_R > 0$. The force enhancements due to point-vortex equilibria are qualitatively similar regardless of the choice of the initial guess. Thus, in the following section, we focus on the point-vortex equilibria for the initial guesses chosen from $\left(\beta^{(1)}, \beta^{(3)}\right)$ and $\left(\beta^{(2)}, \beta^{(3)}\right)$. These cases are of particular significance, since they yield the stationary point vortices entrapped behind the two plates.

(*b*) *Fixed point vortices for* $s = 0.6$ *and various* ϕ

We change the inclined angle ϕ of the two plates separated by the fixed distance $s = 0.6$. We observe how the loci of the point-vortex equilibria change with respect to ϕ when the initial guesses of the Brownian ratchet scheme are chosen from the grid points in $\left(\beta^{(2)}, \beta^{(3)}\right)$. Figure 8(b) shows a series of the loci connected to the leading edge of the right plate for $\phi = 0.4, 0.5, \ldots, 1.0$, while their corresponding loci behind the left plate and their enlarged plots are shown in Figure 8(a).

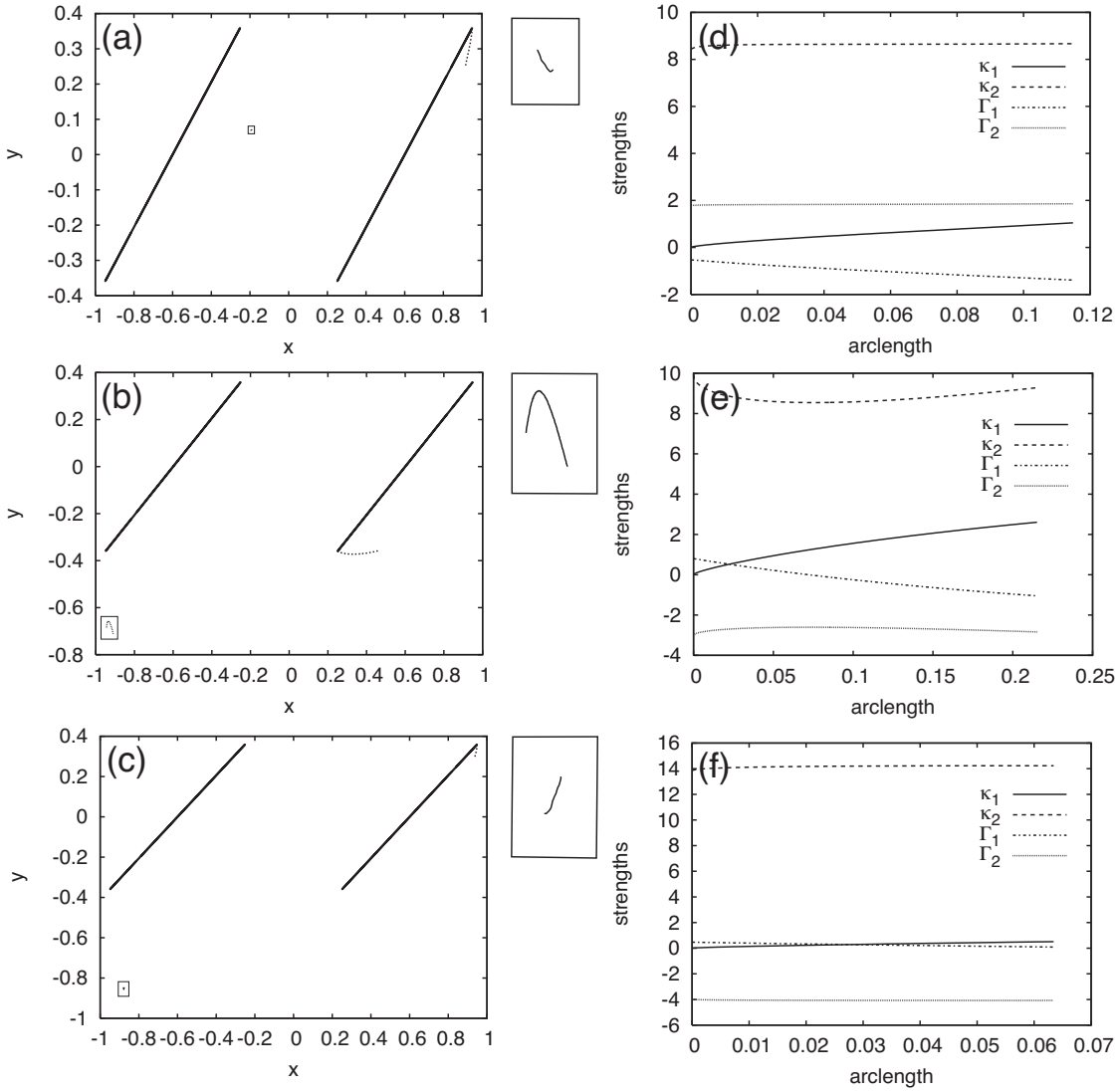

Figure 6. Loci of the point-vortex equilibria for $s = 0.6$ and $\phi = 0.8$ computed by the Brownian ratchet scheme for the initial guesses chosen from (a) $\left(\beta^{(1)}, \beta^{(3)}\right)$, (b) $\left(\beta^{(2)}, \beta^{(4)}\right)$ and (c) $\left(\beta^{(1)}, \beta^{(4)}\right)$. In each plot, the left small locus is surrounded by the rectangle to locate it easily and its enlarged plot is also shown on the right of the figure. Their corresponding vortex strengths κ_1, κ_2 and the round-plate circulations Γ_1, Γ_2 are plotted in (d), (e) and (f) respectively.

As ϕ increases, the right locus moves with the plate and its profile remains similar. On the other hand, the left locus moves in the negative x-direction up to $\phi = 0.7$, then it goes back in the positive x-direction for $\phi \geq 0.8$.

For $\phi \geq 1.2$, the Brownian ratchet scheme provides us with another series of point-vortex equilibria. The left loci with their enlarged plots and the right loci for $\phi = 1.2, 1.3, 1.4$ are shown in Figure 9(a) and 9(b) respectively. The right locus tends to lie along the right plate, while the left small locus is away from the left plate as ϕ increases. We plot in Figure 10(a) and (b) the force enhancements ΔF_L and ΔF_R evaluated for the loci shown in Figure 8 and Figure 9 respectively. Since we observe $\Delta F_L < 0$ and $\Delta F_R > 0$ in both cases, the downward force and the counter-clockwise rotation are enhanced by the stationary point vortices. Figure 10(a) shows that, for the loci in Figure 8, the enhancement of the downward force becomes stronger as the right point vortex gets away from the leading edge for all ϕ. The enhancement of the rotational force

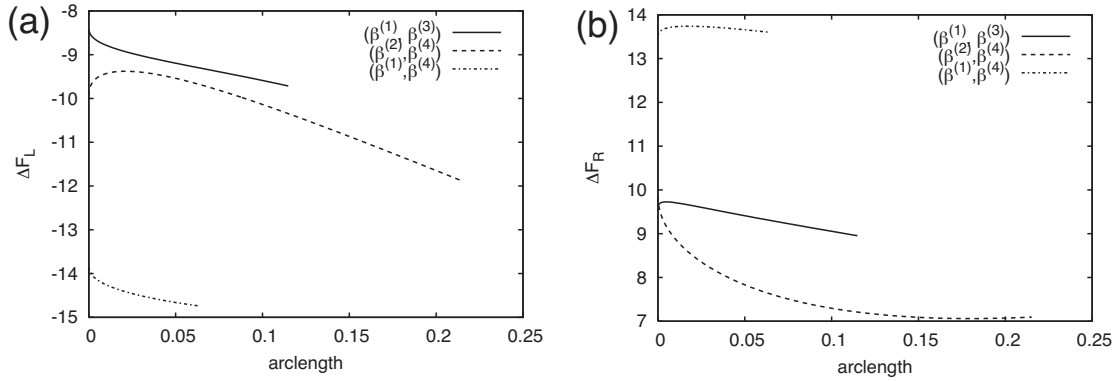

Figure 7. (a) Plots of the lift enhancement ΔF_L. (b) Plots of the rotational force enhancement ΔF_R. They are computed for the point-vortex equilibria shown in Figure 6. The initial guess for the Brownian ratchet scheme is chosen from the grid points in $\left(\beta^{(1)}, \beta^{3}\right)$, $\left(\beta^{(2)}, \beta^{(4)}\right)$ and $\left(\beta^{(1)}, \beta^{(4)}\right)$.

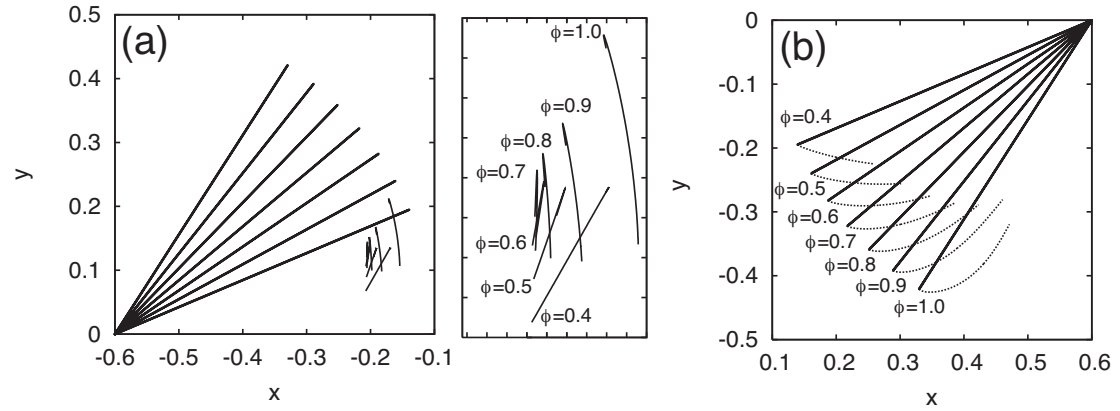

Figure 8. Loci of the point-vortex equilibria for $s = 0.6$ and $\phi = 0.4$, 0.5, 0.6, 0.7, 0.8, 0.9, 1.0. They are computed by the Brownian ratchet scheme with the initial guesses in $\left(\beta^{(2)}, \beta^{(3)}\right)$. (a) Loci behind the left plate (left) and their enlarged plots (right). (b) Loci connected to the leading edge of the right plate.

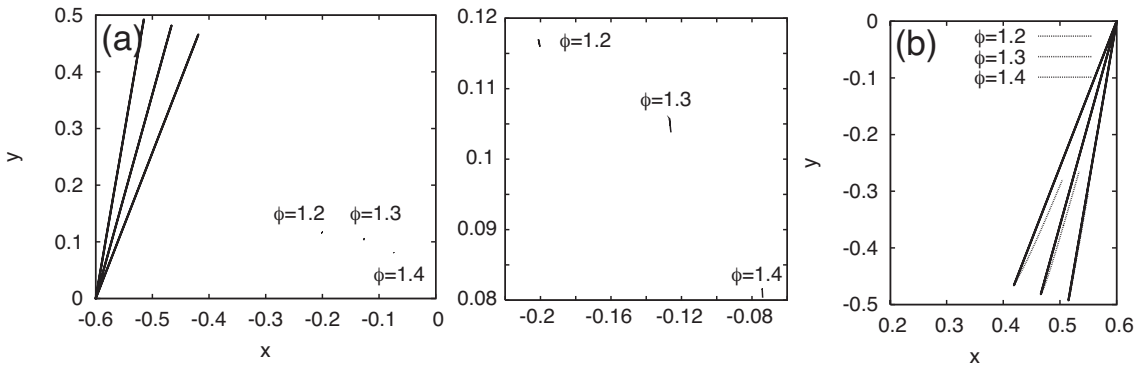

Figure 9. Loci of the point-vortex equilibria for $s = 0.6$ and $\phi = 1.2$, 1.3, 1.4. The Brownian ratchet scheme uses the initial guesses in $\left(\beta^{(2)}, \beta^{(3)}\right)$. (a) Loci behind the left plate and their enlarged plots. (b) Loci connected to the leading edge of the right plate.

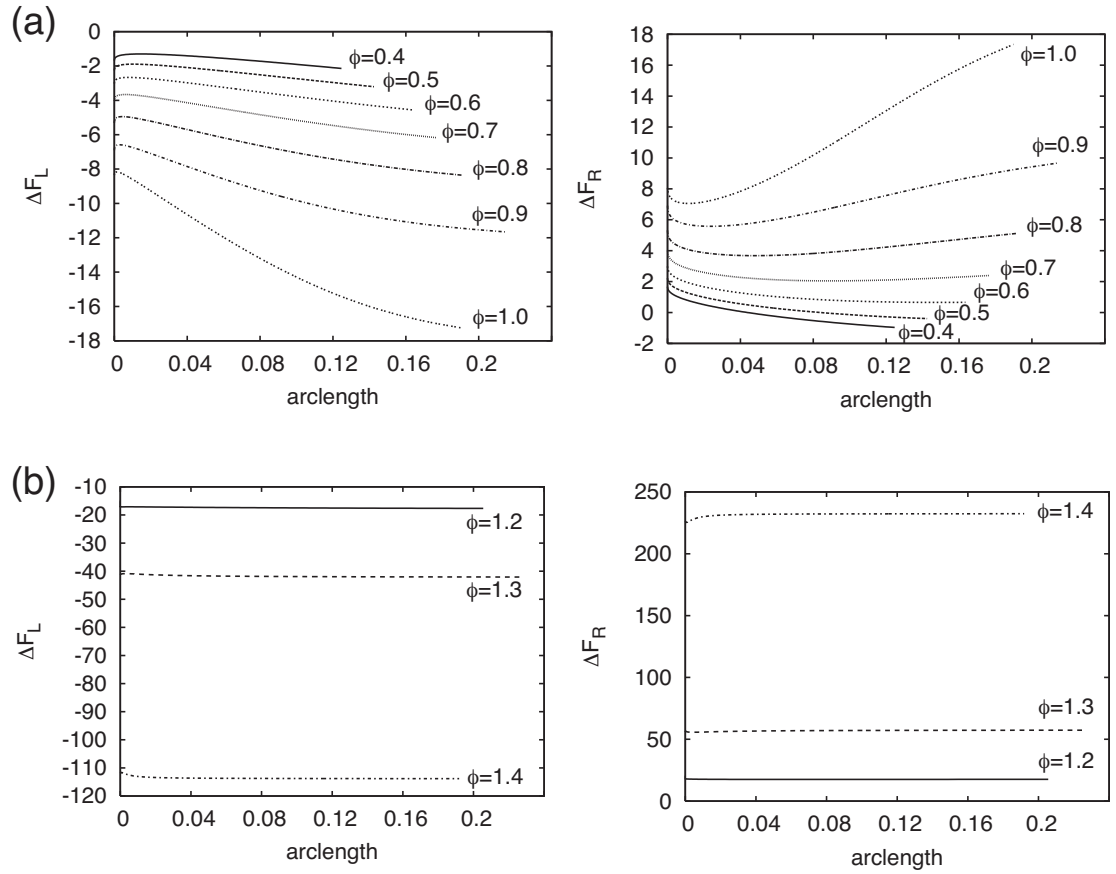

Figure 10. (a) Force enhancements ΔF_L and ΔF_R due to the point-vortex equilibria shown in Figure 8. (b) Force enhancements due to the point-vortex equilibria shown in Figure 9.

becomes the maximum when the right point vortex is at the leading edge for $\phi \leq 0.7$, whereas it gets stronger as the point vortex is away from the edge for $\phi \geq 0.8$. For the loci in Figure 9, the force enhancements stay almost at same values, which are stronger than those for $\phi = 0.4, \ldots, 1.0$ as we see in Figure 10(b)

We show the loci of the point-vortex equilibria when the Brownian ratchet scheme starts with the initial guesses in $\left(\beta^{(1)}, \beta^{(3)}\right)$. Figure 11(a) and (b) are the loci for $\phi = 0.4, \ldots, 1.0$ and those for $\phi = 1.2, \ldots, 1.4$ respectively. In both cases, the right locus joins the trailing edge of the plate. On the other hand, the left small locus moves clockwise for $\phi = 0.4, \ldots, 1.0$, whereas it moves away from the plate for $\phi = 1.2, \ldots, 1.4$ as ϕ increases. The force enhancements due to the point-vortex equilibria are downward and counter-clockwise, i.e., $\Delta F_L < 0$ and $\Delta F_R > 0$, as plotted in Figure 12(a) for $\phi = 0.4, \ldots, 1.0$ and in Figure 12(b) for $\phi = 1.2, \ldots, 1.4$. As ϕ gets larger, we have stronger force enhancements of the downward force and the counter-clockwise rotation.

(*c*) *Fixed point vortices for various s*

Let us now fix the inclined angle $\phi = 0.8$ and change the distance s of the two plates. Figure 13(a) shows the loci of the point-vortex equilibria for $s = 0.6$, 0.8 and 1.0, which are obtained by the Brownian ratchet scheme for the initial guesses chosen from $\left(\beta^{(2)}, \beta^{(3)}\right)$. Both of the loci move in the same direction as the two plates. The profile of the right locus connected to the trailing edge is unchanged, while the arclength of the left locus gets smaller. As a matter of fact, it gets harder to obtain the point-vortex equilibria with the Brownian ratchet scheme for larger s. This is because, as $s \to \infty$, the interaction between the two plates gets weaker and thus the flow profiles in the neighborhood of these two plates become independent with each other.

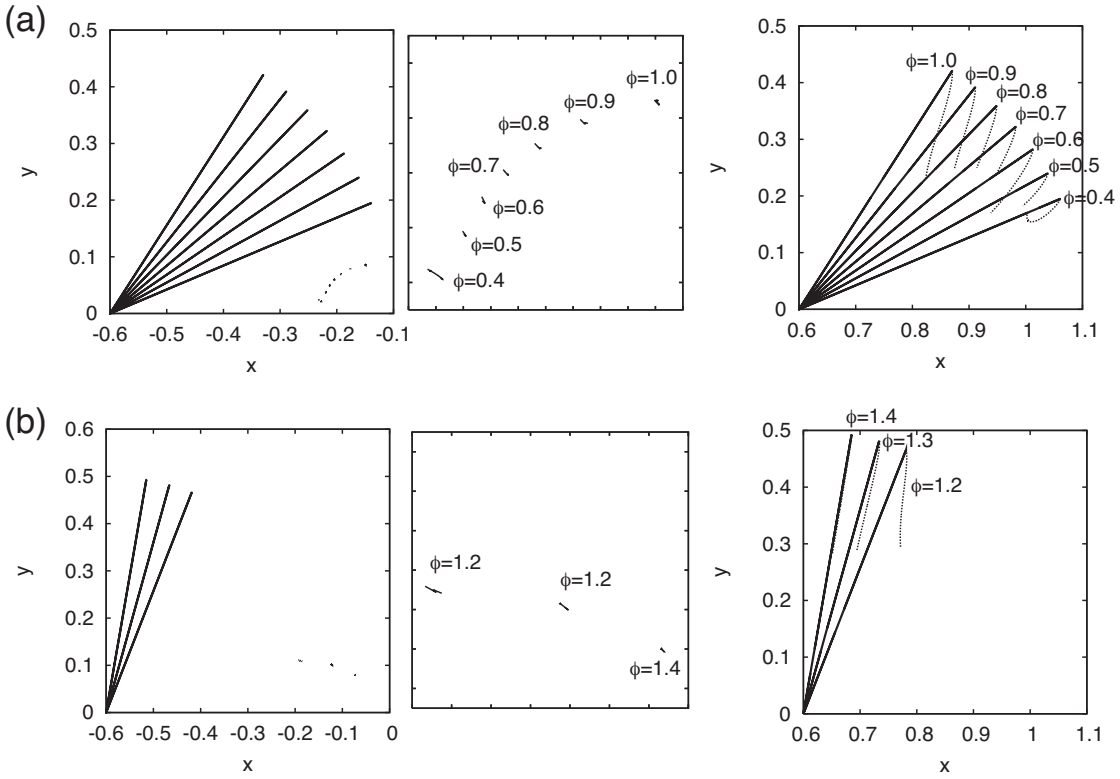

Figure 11. Loci of the point-vortex equilibria for $s = 0.6$ and various ϕ, which are computed by the Brownian ratchet scheme starting with the initial guesses in $\left(\beta^{(1)}, \beta^{(3)}\right)$. (a) Left loci and their enlarged plots (left), and the right loci (right) for $\phi = 0.4, \ldots, 1.0$. (b) Left loci and their enlarged plots (left), and the right loci (right) for $\phi = 1.2$, 1.3 and 1.4.

Consequently, the flow around the right plate tends to that around a single plate with the Kutta conditions to be imposed at its leading and trailing edges simultaneously, for which there is no vortex equilibrium around the plates as discussed in Saffman & Sheffield (1977). On the other hand, since the flow profile in the vicinitiy of the left plate tends to what Saffman & Sheffield (1977) considered as $s \to 0$, we expect the convergence to the locus attached to the trailing edge of the left plate. However, we have obtained no left locus like this for the initial guess of the Brownian ratchet scheme explained in § 3. It may be possible to obtain such a left locus when we use a different procedure to choose initial guess of the Brownian ratchet scheme, which will be confirmed elsewhere in the near future. The force enhancements due to the point-vortex equilibria are plotted in Figure 13(b), which indicates that the downward force and the counter-clockwise rotation are enhanced. We have stronger force enhancements for larger s, but these point-vortex equilibria hardly exist as s increases.

6. Conclusion and discussion

We have considered a potential flow in a two-dimensional unbounded domain with two parallel plates, in which we search stationary configurations of two point vortices around the plates in the presence of the uniform flow. We solve numerically the equations for the point-vortex equilibria with the Kutta condition imposed at the edges of the plates, which are described in terms of the elliptic functions. As the numerical method, we have proposed a linear algebraic algorithm with the Brownian random walk, called the Brownian ratchet scheme. The numerical algorithm allows us to compute the loci of the point-vortex equilibria in the doubly connected domain effectively.

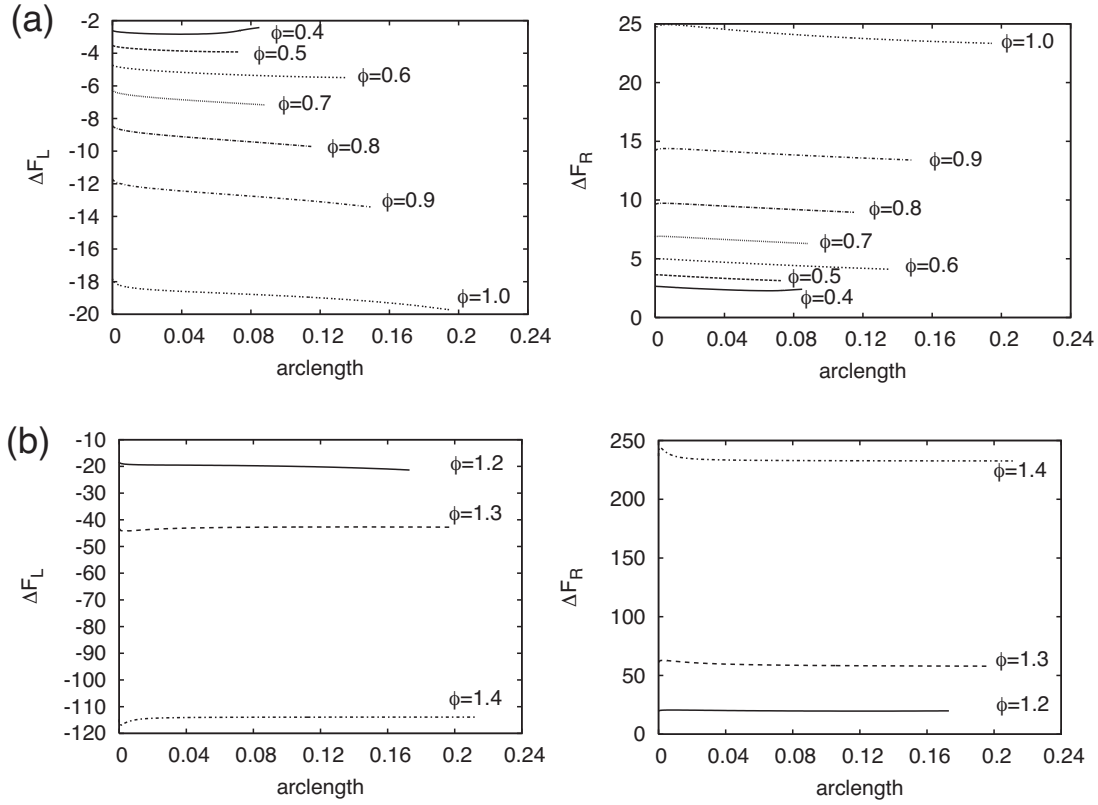

Figure 12. (a) Plots of the force enhancements ΔF_L and ΔF_R by the point-vortex equilibria in Figure 11(a). (b) Plots of the force enhancements by the point-vortex equilibria in Figure 11(b).

The geometric parameters are the distance s between the two plates and their inclined angle ϕ. When the distance is $s = 0.6$, we obtain the two series of the loci of the point-vortex equilibria for $\phi = 0.4, \ldots, 1.0$ and for $\phi = 1.2, \ldots, 1.4$, in which one locus is connected to the edge of the right plate and the other locus exists between the two plate. Furthermore, introducing the rigid rod model, the force acting on the two parallel plates is investigated, which shows that the downward force and the counter-clockwise rotation are enhanced by all the point-vortex equilibria obtained in the present paper. The force enhancements tend to be larger as the inclined angle ϕ tends to vertical. We also observe that the force enhancements get stronger as the distance s increases, although the point-vortex equilibria hardly exist for large s.

Let us discuss possible future extensions of the present study. First, it is important to investigate the stability of the point-vortex equilibria. However, once the stationary point vortices are perturbed, we need to generate more point vortices from the trailing edges so that the Kutta condition is satisfied for all time. Second, it is possible to consider stationary configurations of two vortex-sinks around the two plates as Mourtos & Brooks (1996). Finally, the present study suggests that the point-vortex equilibria enhance the rotational force on the two parallel plates. However, the conclusion is partial when one wants to apply it to the design problem for the efficient wind turbine with the vertical multiple blades, since we assume that the configuration of the two plates is just parallel and the Kutta condition is imposed at the three edges ζ_1, ζ_2 and ζ_3. There may be other optimal configurations of the two plates with stationary point vortices enhancing the rotational force more effectively if we consider the Kutta condition at different edges or we change the configuration of the two plates more flexibly. In order to change the configuration of the two plates arbitrarily, we need to construct the conformal mapping from the canonical annulus to the target domain. However, we must note that the Brownian ratchet scheme presented in this paper still works. These extensions will be reported in the future.

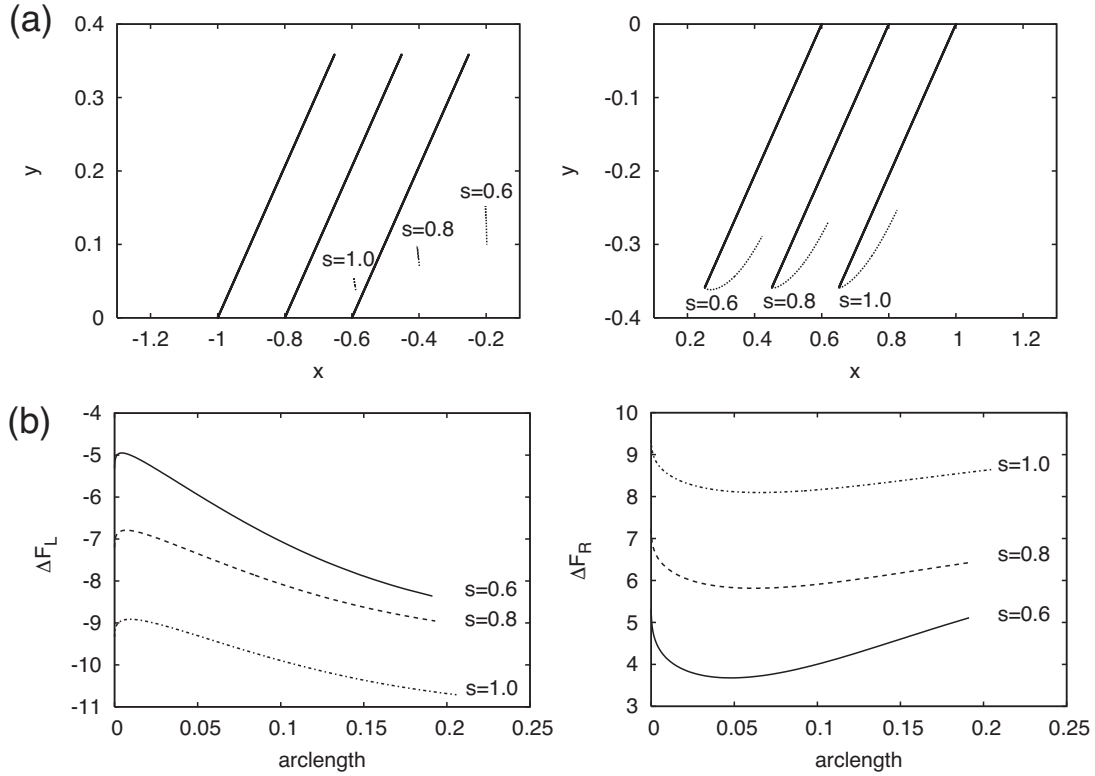

Figure 13. (a) Loci of the point-vortex equilibria for $s = 0.6$, 0.8 and 1.0. The upper half of the left plates and the lower half of the right plates are plotted. The inclined angle of the two plates is fixed to $\phi = 0.8$. The initial guess of the Brownian ratchet scheme is chosen from $\left(\beta^{(1)}, \beta^{(3)}\right)$. (b) Force enhancements ΔF_L and ΔF_R due to the point-vortex equilibria.

Acknowledgements

The author would like to show my gratitude to Professor Darren Crowdy for introducing the present problem and for providing me with the data required to compute the conformal mapping. This study is partially supported by JSPS grant and #21340017, JST PRESTO and JST CREST. I would also thank the referees for their fruitful comments and suggestions.

References

Crowdy, D. & Marshall, J. 2005 Analytic formulae for the Kirchhoff-Routh path function in multiply connected domains. *Proc. Roy. Soc. A* **461**, 2477–2501.

Crowdy, D. 2006 Calculating the lift on a finite stack of cylindrical aerofoils. *Proc. Roy. Soc. A*, **462**, 1387–1407.

Crowdy, D. & Marshall, 2006 Conformal mappings between canonical multiply connected domains. *Comput. Methods Funct. Theory* **6**, 59–76.

Crowdy, D. 2010 A new calculus for two dimensional vortex dynamics. *Theor. Comput. Fluid Dyn.* **24**, 9–24. (doi:10.1007/s00162-009-0098-5)

Huang, M.-K. & Chow, C.-Y. 1981 Trapping of a free vortex by Joukowski airfoils. *AIAA paper* **82-4059**.

Hummel, D. 1978 On the vortex formation over a slender wing at large angles of incidence. *AGARD CP-247*, **15**.

Kruppa, E. W. 1977 A wind tunnel investigation of the Kasper vortex concept. *AIAA paper* **77-310**.

Mourtos, N. J. & Brooks, M. 1996 Flow past a flat plate with a vortex/sink combination. *J. Appl. Mech.* **63**, 543–550.

Newton, P. K. & Chamoun, G. 2007 Construction of point vortex equilibria via Brownian ratchets. *Proc. Roy. Soc. A* **463**, 1525–1540.

Rossow, V. G. 1977 Lift enhancement by an externally trapped vortex. *AIAA paper* **77-672**.

Saffman, P. G. & Sheffield, J. S. 1977 Flow over a wing with an attached free vortex. *Stud. Appl. Math.* **57**, 107–117.

Saffman, P. G. 1992 *Vortex Dynamics.* Cambridge, UK: Cambridge Univ. Press.

Sakajo, T. 2009 The N-vortex problem in multiply connected domains. *Proc. Roy. Soc. A* **465**, 2589–2611.

Trefethen, L. N. & Bau III, D. 1997 *Numerical linear algebra.* Philadelphia, PA: SIAM Publishing.

Walton, D. 1974 A brief wind tunnel test of the Kasper aerofoil. *Soaring* **38**, 26–27.

Zannetti, L. 2006 Vortex equilibrium in flows past bluff bodies. *J. Fluid Mech.* **562**, 151–171.